Ultra-low emission combustion of diesel-coconut biodiesel fuels by a Mixture Temperature-Controlled Combustion mode

Viktor Józsa[a,*], Gyöngyvér Hidegh[a], Attila Kun-Balog[a], Jo-Han Ng[b], Cheng Tung Chong[c]

[a] Budapest University of Technology and Economics, Faculty of Mechanical Engineering, Department of Energy Engineering, 1111 Budapest, Műegyetem rkp. 3., Hungary

[b] Faculty of Engineering and Physical Sciences, University of Southampton Malaysia (UoSM), 79200 Iskandar Puteri, Johor, Malaysia

[c] China-UK Low Carbon College, Shanghai Jiao Tong University, Lingang, Shanghai 201306, China

Abstract

Liquid fuels are likely to remain the main energy source in long-range transportation and aviation for several decades. To reduce our dependence on fossil fuels, liquid biofuels can be blended to fossil fuels – or used purely. In this paper, coconut methyl ester, standard diesel fuel (EN590:2017), and their blends were investigated in 25 V/V% steps. A novel turbulent combustion chamber was developed to facilitate combustion in a large volume that leads to ultra-low emissions. The combustion power of the swirl burner was 13.3 kW, and the air-to-fuel equivalence ratio was 1.25. Two parameters, combustion air preheating temperature and atomizing air pressure were adjusted in the range of 150–350 °C and 0.3–0.9 bar, respectively. Both straight and lifted flames were observed. The closed, atmospheric combustion chamber resulted in CO emission below 10 ppm in the majority of the cases. NO emission varied between 60 and 183 ppm at straight flame cases and decreased below 20 ppm when the flame was lifted since the combustion occurred in a large volume. This operation mode fulfills the 2015/2193/EU directive for gas combustion by 25%, which is twice as strict as liquid fuel combustion regulations. The 90% NO emission reduction was also concluded when compared to a lean premixed prevaporized burner under similar conditions. This favorable operation mode was named as Mixture Temperature-Controlled (MTC) Combustion. The

chemiluminescent emission of lifted flames was also low, however, the OH* emission of straight flames was clearly observable and followed the trends of NO emission. The MTC mode may lead to significantly decreased pollutant emission of steady-operating devices like boilers, furnaces, and both aviation and industrial gas turbines, meaning an outstanding contribution to more environmentally friendly technologies.

Keywords: biodiesel; emission; spectroscopy; swirl combustion; coconut; liquid fuel

* Corresponding author. Email: jozsa@energia.bme.hu

1. Introduction

The challenge of our decade is reaching sustainability. A dramatic change is required for land-based energy generation for the transition of fossil fuel heavy primary energy carriers to renewable energy sources [1]. Regardless that batteries went through rapid and spectacular development in the past decade, the state-of-the-art Li-ion cells offer gravimetric energy density only in the range of 1 kJ/kg [2] and other, high energy density batteries under research perform below 5 kJ/kg [3,4]. In comparison, the presently investigated standard diesel fuel (D, EN590:2017) offers 43 MJ/kg lower heating value while that of the coconut methyl ester (CME) is 35.15 MJ/kg. As a consequence, all the long-range passenger aircraft on the horizon will feature highly efficient gas turbines [5,6]. The interest in advanced technologies is pushed by the rapid growth of the aviation industry, which is a few percents each year [7,8].

Among the potential alternative fuels for power and transportation sector, biodiesel stands out [9,10]. The transesterified fatty acids can be either saturated or unsaturated [11]. Alongside with the feedstock, the physical properties are significantly affected, from which the pour point is a severe limitation in many applications and in cold climate [9]. Although biodiesel is inherently oxygenated, the overall quality is still resembling those of diesel, making it a compatible blending fuel for existing combustion systems.

At present, the primary interest for biofuel applications is in the transportation sector. Biodiesel is blended to commercial diesel fuel, according to regulations in many countries, such as those in, e.g., Malaysia and Hungary (B7), Indonesia (B20), and Brazil (B8). This explains the growing trend of biodiesel production globally [12], driven by renewable energy policies to reduce the dependency on fossil fuel. Most of the biodiesel is produced from first-generation feedstock, i.e. edible oil seeds, although further emphasis is placed on the use of non-food based feedstock, such as agricultural wastes, industrial biowastes, and non-food based energy crops, as stipulated in the Renewable Energy Directive (RED) II [13]. The

perspectives of aviation biofuel production for the EU are summarized by Prussi et al. [8], which was motivated by the push for reduced greenhouse gas emissions in aviation [14,15]. In this industry, the processing method of hydroprocessed esters and fatty acids (HEFA) has been certified as one of the biojet fuel production pathway by ASTM International [15] to improve the oxidative stability and heating value of the biojet fuel [16]. The KLM airline is already operating a daily intercontinental flight using HEFA [17], demonstrating similar combustion properties compared to conventional jet fuels [18].

In the power generation industry, biodiesel is an efficient substitute of fossil fuels while achieving the benefit of lower NO_X emissions [19]. The continuous swirl burning mode of the gas turbine combustor has made it feasible to be adopted in the fuel-flexible micro gas turbines [20]. Recent studies have shown that the swirling flame behavior of biodiesel is somewhat similar to diesel despite the visibly of different flame spectral characteristics [21]. The coconut biodiesel was reported to emit the lowest NO and CO compared to soy and palm biodiesels [22], attributable to the fuel chemistry effect that plays an important role in the pollutant formations, i.e., degree of unsaturation of the biofuel.

The pollutant emission of aero engines was spectacularly cut back by the end of the last century [23]. Non-premixed combustion mode is characterized by high flame stability and also excessive NO_X emission [24]. Consequently, various lean flame concepts were developed and put into practice to provide a homogeneous temperature profile at the turbine inlet [25]. The list includes rich burn-quick quench-lean burn (RQL), lean premixed prevaporized (LPP) swirl, and catalytic combustors [26]. RQL combustion offers the best of two worlds: the rich flame root helps flame stabilization while the residence time is insufficient for thermal NO_X formation [27]. However, the flame is less homogeneous in the lean side, hence, the NO_X emission of this concept falls behind that of LPP burners, which feature a swirler for flame stability [28]. To further cut NO_X emissions, increased combustion air flow is required, pushing

LPP to the lean blowout limitation where thermoacoustic oscillations endanger the operation [29]. Other approaches are using more but smaller burners [30] and flow control of concentric swirlers [31]. Catalytic combustion was a promising idea to provide a homogeneous flue gas stream, but the excessive unburnt fuel due to the large wall surface areas hampered the spreading of this concept [32]. The most straightforward approach to eliminate NO_X emission is oxyfuel combustion [33]. Since efficient oxygen extraction from the atmosphere is not solved yet, hence, it is not a competitive solution for land-based applications. Nevertheless, this concept makes carbon capture and storage technologies easier since the flue gas contains only carbon dioxide and water vapor [34].

The next advancement in combustion technology was flameless combustion, which solves the high flame temperature problem, hence characterized by even lower thermal NO_X formation than LPP burners by recirculating a portion of the flue gas [35]. This concept works flawlessly in a laboratory environment, nevertheless, the efficient and reliable flue gas recirculation still has to be solved at practical scales [36]. Similar to the RQL concept, air staging provided promising results in NO_X emission reduction in swirl burners [37–39], however, the perfectly homogeneous fuel-air mixture could lead to the optimal result. Mixture control was in the focus of hypersonic vehicles [40] to provide a proper heat release pattern, and more recently, in internal combustion engines [41]. This is also a key momentum of the present concept with a difference of average flow velocity in the range of 1 m/s instead of a few hundred m/s. Motivated by the reviewed combustion concepts above, a novel swirl burner concept was designed with a central plain-jet airblast atomizer, detailed in Subsection 2.1. The cold atomizing air delays the ignition of the mixture in the central region, which leads to ultra-low NO_X emission. The observed flame volume was approximately 150×150×150 mm on average which means 4 MW/m^3 volumetric heat release rate. This combustion concept can be best characterized by Mixture Temperature-Controlled (MTC) combustion mode, which is a

novel variant of RQL combustion since mixture ignition is delayed at the center by controlling the temperature instead of the fuel-air mixture. To see this operation mode, see the supplementary video records in the web version of this paper. A similar concept in industrial scale was presented by Wang et al. [42] in a retrofit of a utility boiler.

The novelty of the present study is the following. To reduce our dependence on fossil fuels, the renewable content of conventional petroleum-based fuels can be increased. Hence, D, CME, and their blends were investigated in a novel, MTC burner. The liquid fuels were atomized by a plain-jet airblast atomizer, and the combustion air was preheated to various temperatures. Since the cold atomizing air flow occupies the central region, the combustion can be delayed, leading to lifted flames. Hence, combustion occurs in a large volume, consequently, extremely low NO emission can be achieved.

2. Materials and methods

The used combustion chamber is detailed in this section first, also discussing the measurement uncertainties, swirl, and average air temperature since atomizing air also enters the combustion chamber beside the preheated combustion air. Secondly, the fuel properties are discussed for D, CME, and their blends. Thirdly, the estimated spray characteristics are evaluated.

2.1 Experimental setup

The schematic of the atmospheric test rig is shown in Fig. 1. The liquid fuel was delivered from a pressurized tank to maintain a smooth flow rate, measured by an Omega FPD3202 positive displacement flow meter. It was calibrated for diesel fuel and CME with a result of < 2.7% uncertainty at 95% level of significance. The combustion power was 13.3 kW, and the air-to-fuel equivalence ratio was 1.25 in all cases. Atomization of the fuel was

performed by a plain-jet airblast atomizer. The atomizing gauge pressure, p_g, was varied between 0.3 bar and 0.9 bar in 0.15 bar steps. The atomizing air flow rate was considered during the adjustment of the combustion air flow rate to ensure the identical equivalence ratio. More details on the atomizer characteristics are discussed in Subsection 2.3. The volume flow rate of atomizing air was measured by a pre-calibrated Omega FMA1842A flow meter. Its uncertainty was 1 liter/min in the 20-100 liter/min operating range. The combustion air was delivered by a frequency-controlled side channel blower. The flow rate was measured by a pre-calibrated Fuji Electric FWD050D2-A52 ultrasonic flow meter which had a 5% uncertainty of the reading. The combustion air was preheated to the desired temperature by a PID-controlled, 11.8 kW Herz PH92 electric air heater in the range of t_{ca} = 150-350 °C in 50 °C steps.

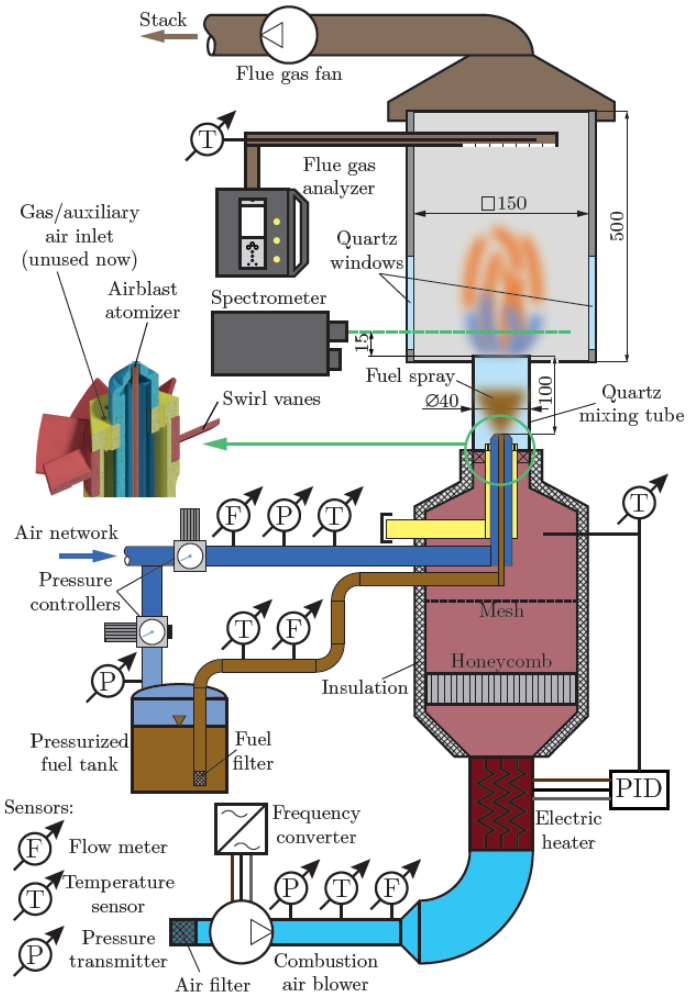

Figure 1. The combustion test rig.

A Testo 350 flue gas analyzer was used to measure the CO and NO content. Since this device features an O_2 sensor, a constant 4.2% O_2 level was measured and no correction was required to have a similar O_2 basis for the pollutants. The uncertainty of the CO, NO, and O_2 sensors were 3 ppm, 2 ppm, and 0.2 V/V%, respectively. The spectrometer was manufactured by OpLab Kft. and featured a Hamamatsu S3904-1024Q nMOS 1024 pixel photosensor. The spectrum range was 260-580 nm, resulting in a 0.3125 nm spectral resolution. A Fujifilm HS10 camera in a fixed position was recording three flame images at each operating point for visual evaluation, placed next to the spectrometer. All the temperature sensors were B-class Pt100 resistance thermometers (0.4 °C accuracy), except for the combustion air upstream and the flue

gas measurements where standard K-type thermocouples (accuracy is max(2.2,t[°C]×0.0075), which is 5.6 °C at 745 °C) were installed due to the elevated temperatures. Even though the flue gas temperature measurement accuracy seems excessive, the measurement error is similar at high temperatures. Hence, the temperature differences are much more accurate.

The annulus at the 45° swirl vane had a 40 mm outer and 21 mm inner diameter, generating a geometric swirl number, S = 0.787 [28]. The theoretical air demand for 13.3 kW combustion power and 4.2% excess O_2 is 16 kg/h which is the sum of atomizing and combustion air flow rates. At p_g = 0.3 bar, the atomizing air flow rate was varied between 2.13 kg/h (at t_{ca} = 350 °C) and 2.37 kg/h (at t_{ca} = 150 °C), depending on the combustion air preheating temperature since the whole rig reached higher temperatures and the hydraulic losses increased. The atomizing air flow rates were varied between 5.45 kg/h and 6.1 kg/h at p_g = 0.9 bar.

2.2 Fuel properties

The fuels used in the present study are the standard Euro 5 diesel and CME, which was produced in-house via the transesterification process. The coconut oil was first heated up to 60 °C before mixing with methanol and potassium hydroxide (KOH) at the ratio of 114:50:1 (oil:methanol:KOH) by mass. The mixture was stirred for 2 h using a magnetic stirrer to ensure a homogenous reaction at 60 °C to convert the fatty acids into methyl esters. Subsequently, the end product was left to separate into two distinct layers, i.e. biodiesel and glycerol. The latter was removed by decanting the mixture. The remained biodiesel was heated up to 120 °C for 4 hours in an ordinary oven, open to the atmosphere to vaporize the diluted methanol and water. Characterization of the biodiesel was carried out via gas chromatography (Agilent 7820A) based on the EN 14103 standard. The production yield was 96.9%. The CME is mainly composed of ~93% saturated fatty acids, as shown in Table 1.

Table 1. Fatty acid composition of the CME.

Acid	Structure	Composition [%]
Caprylic acid	C8:0	6.78
Capric acid	C10:0	5.61
Lauric acid	C12:0	51
Myristic acid	C14:0	18.51
Palmitic acid	C16:0	9.26
Stearic acid	C18:0	1.66
Oleic acid	C18:1	6.06
Linoleic acid	C18:2	1.12

The fuel properties for the estimation of atomization characteristics and maintaining the 13.3 kW combustion power are shown in Table 2. The lower heating value, *LHV*, was estimated based on [43], the rest of the properties of diesel fuel were measured, while the other parameters for the CME and the blends were estimated based on Refs. [44–47]. The density was measured using a standard borosilicate 10 ml pycnometer, the kinematic viscosity by a Cannon-Fenske-type viscometer; both of them were performed in a temperature-controlled oil bath. The surface tension was measured by the Wilhelmy plate method, also in a tempered environment. The CME is noted with B100, while the other blends are referred to as BX, where X is the volumetric CME content.

Table 2. Relevant physical properties of the fuels.

Fuel	D	B25	B50	B75	B100
LHV [MJ/kg]	43	40.95	38.91	36.86	35.15
Fuel flow rate [kg/h]	1.11	1.17	1.23	1.30	1.44
Density [kg/m^3]	820	832	844	856	868
Kinematic viscosity [mm^2/s]	2.53	2.74	2.95	3.16	3.37
Surface tension [mN/m]	25.6	26.05	26.5	26.95	27.40

2.3 Liquid fuel atomization

The fuel pipe of the plain-jet airblast atomizer had 1.5 mm outer and 1.2 mm inner diameter, and the diameter of the air nozzle was 2.2 mm. Based on our previous work [48] on high-velocity airblast atomization, estimated Sauter Mean Diameters, *SMD*, at all conditions

are summarized in Table 3. The corresponding air-to-liquid mass flow rates, *ALR*, were in the range of 1.67 (B100 at p_g = 0.3 bar)–5.16 (D at p_g = 0.9 bar).

Table 3. Estimated *SMD* [µm] at all investigated conditions.

p_g [bar]/Fuel	D	B25	B50	B75	B100
0.3	8.29	9.07	9.88	10.73	11.59
0.45	7.45	8.13	8.84	9.58	10.32
0.6	6.96	7.58	8.23	8.90	9.57
0.75	6.62	7.20	7.80	8.43	9.05
0.9	6.38	6.94	7.51	8.10	8.69

Among the fuel parameters discussed in Table 2, the higher viscosity, surface tension, and liquid flow rate of B100 to diesel fuel resulted in an increase in *SMD*. The other reason why diesel fuel standards allow only a few percent biodiesel is also due to the lower volatility of the latter [49,50]. As a consequence, a fuel spray with high biodiesel content requires more time for complete vaporization. The key combustion parameters are summarized in Table 4, including the Reynolds number, *Re*, at the mixing tube.

Table 4. Overview of the key parameters.

Parameter	Value/range
Combustion power [kW]	13.3
Fuels	D, B25, B50, B75, B100
λ [1]	1.25
t_{ca} [°C]	150–350
Re [1]	6396–8316
p_g [bar]	0.3–0.9
SMD [µm]	8.29–11.59
ALR [1]	1.67-5.16

3. Results and discussion

Due to the unusual swirl numbers and the novel MTC combustion mode, this section starts with a qualitative analysis to present the occurring flame shapes and their characteristics at four distinct p_g and t_{ca} values for all fuels. Then the analysis of chemiluminescent emission is discussed, which is followed by an overall quantitative evaluation, presenting OH* intensity, flue gas temperature, and pollutant emissions.

189

190 *3.1 Flame characteristics*

191 The atomizing air discharge significantly increases the axial thrust, hence, lowers the
192 overall swirl number. Since the swirl number is depending on both p_g and t_{ca}, the results are
193 shown in Fig. 2a. The high atomizing air flow rates decreased S significantly. This is the reason
194 why V-shaped flames were not observed at all which require otherwise $S > 0.52$, based on our
195 previous observations [51]. Also, the average temperature of the sum of combustion air and
196 atomizing air, t_a, was notably affected by the atomizing air flow rate, shown in Fig. 2b. Even
197 though the pressure, volume flow rate, and temperature of the atomizing air was measured, the
198 expansion at the nozzle had to be calculated, assuming adiabatic expansion, adopted from a
199 previous paper on a similar atomizer type [52]. This strong influence of the atomizing air leads
200 to the MTC name of this combustion concept.

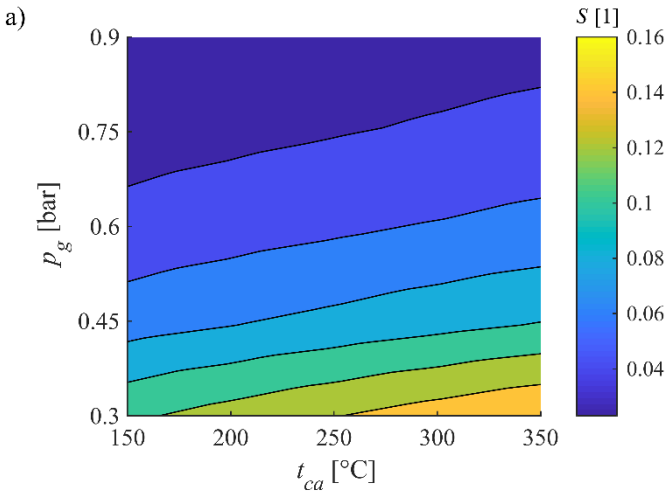

201

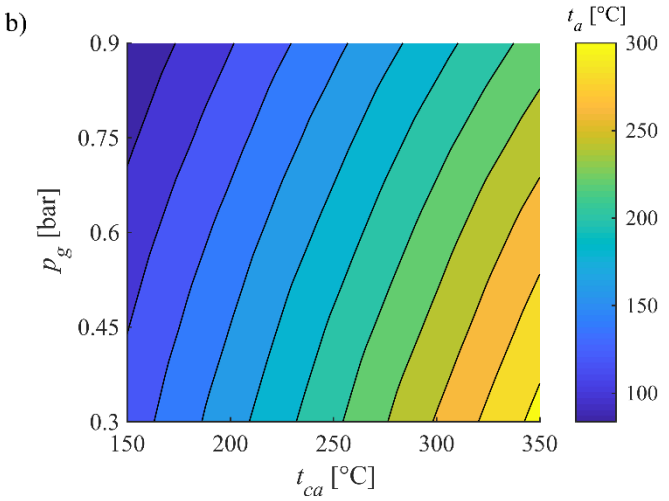

Figure 2. a) swirl number and b) average temperature of the combustion plus atomizing air inlets.

Considering all the measurement setups, two flame shapes were observed during the combustion tests: straight flame and lifted flame, featuring distributed combustion, which is specific to the MTC combustion. Since the conditions resulted in fully turbulent combustion, there were setups where both shapes were observed and a transition occurred between them at about 1 Hz. The observed flame shapes are presented in Fig. 3. Even though the lowest indicated combustion air preheating temperature was 150 °C, lower values were also tested without achieving self-sustaining combustion. In the case of B75 and B100, at least 200 °C preheating temperature was necessary for a stable flame.

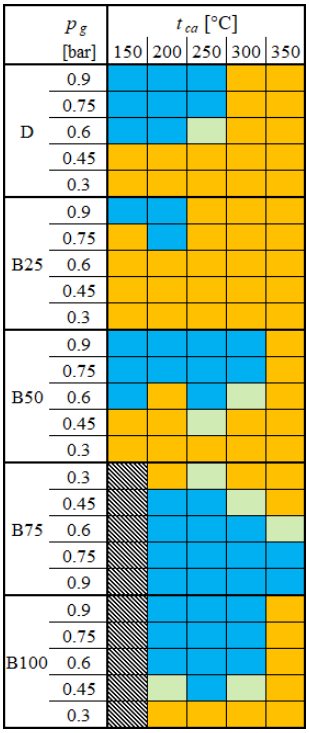

Figure 3. Flame shapes at all the investigated conditions. Orange: straight, blue: distributed (MTC), light green: transitory flames. No stable combustion was observed in the hatched region due to insufficient fuel vaporization.

Four operating points were selected to present the combustion characteristics for visual evaluation, shown in Fig. 4. According to Fig. 3, only straight flames were observed at p_g = 0.3 bar and t_{ca} = 200 °C and 350 °C. This was true for p_g = 0.9 bar and t_{ca} = 350 °C as well, excluding B75 which allows the visual comparison of the effect of both p_g and t_{ca} on the flame. p_g = 0.9 bar and t_{ca} = 200 °C condition was selected to show the MTC combustion mode. The hollow/low-temperature central part was also concluded by Yang et al. [37] and Zhou et al. [38] in the case of the burner upgrade of a coal-fired boiler. The elevated combustion air inlet temperature resulted in more luminous flames in all the cases, and the CME dilution decreases the number of flares. This is more spectacular for B75 and B100, but both B50 and B25 show this characteristic.

The effect of p_g on the flame structure can be evaluated based on the third and fourth columns of Fig. 4; the flame luminosity was lower, and there were no flares present. Even though the estimated *SMD* of D at p_g = 0.3 bar is very close to that of B100 at p_g = 0.9 bar, the

231 resulting flame structures are different as the latter one features no flares unlike the former fuel.
232 Considering that the equivalent air inlet temperature, shown previously in Fig. 2b, which
233 considers both the cooler atomizing air and the combustion air, the opposite results would be
234 intuitively expected, based purely on the boundary and global combustion conditions. The
235 effect of larger droplet sizes, however, is shown in the last column. By increasing the
236 concentration of CME, the flame becomes more luminous as the larger droplets require more
237 time to evaporate, hence, the fuel-air mixture is less homogeneous as the share of the CME is
238 increasing.

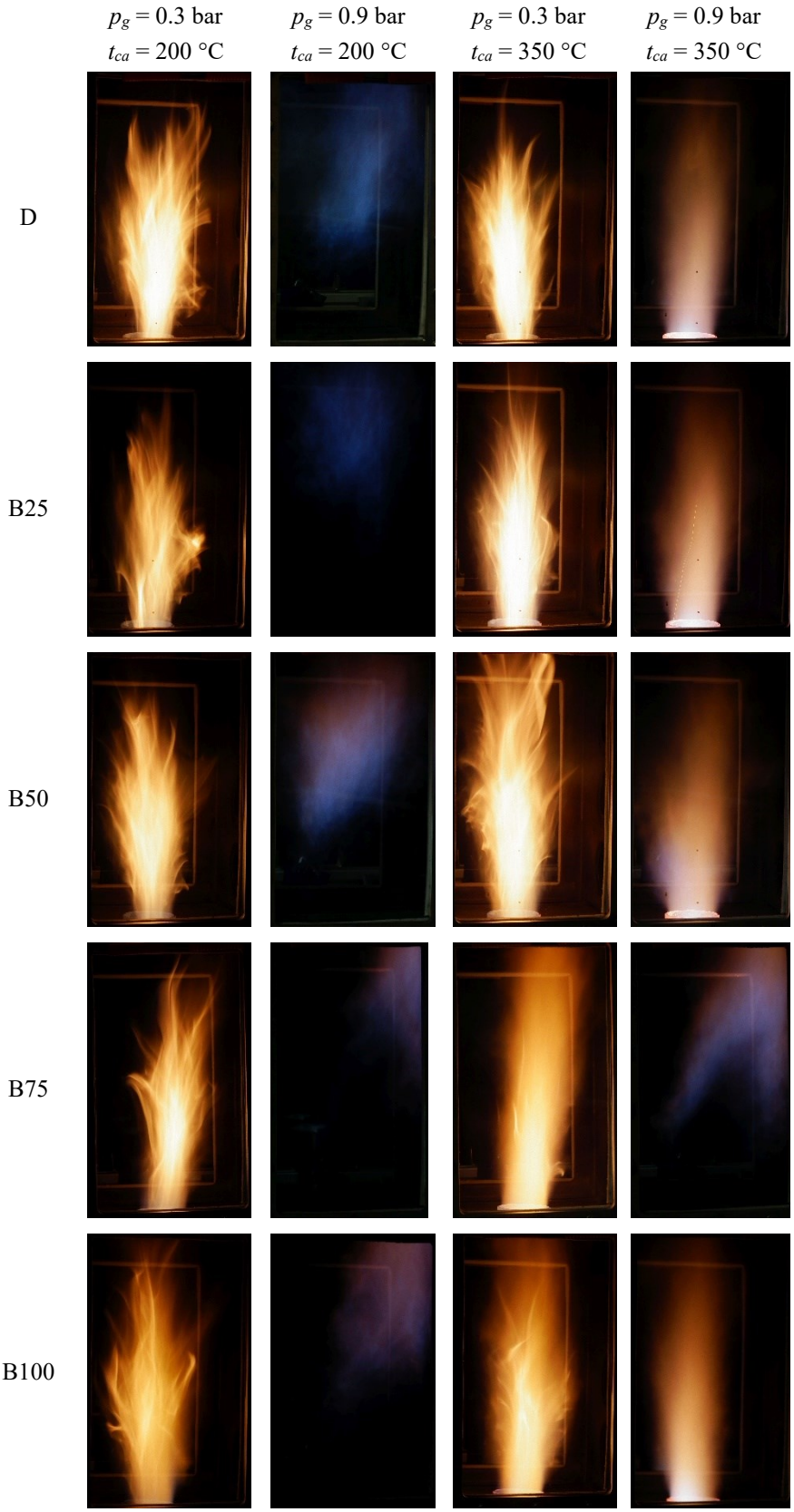

Figure 4. Flame images at various conditions. All the presented, single images were recorded at 1/30 s shutter speed, f/4, and ISO-400. See the supplementary materials for the video files in FullHD at 30 frames/second.

The distributed combustion is characterized by very low luminosity and principally blue color in the case of D and B25. Fuels with higher CME content feature purple color which is the evidence of different reaction pathways due to the fuel-bonded oxygen, also observed by Chong et al. by utilizing sunflower biodiesel [21]. Note that the asymmetry of flames, i.e., they are leaning right, is attributed to the cooled microphone socket on the left side of the combustion chamber – the acoustical data is omitted in the present study for the sake of conciseness. This effect is more spectacular in the case of distributed combustion mode where the heat release rate is lower, and hence the effect of wall temperature on the flame shape is significant. Overall, the flame images show a marginal difference between the fuel types which is an expected result since the physical properties of the biodiesel are close to that of standard diesel fuel.

3.2 Chemiluminescent and pollutant emissions and flue gas temperature

The chemiluminescence spectra of all fuels at p_g = 0.3 bar, t_{ca} = 200 °C and p_g = 0.9 bar, t_{ca} = 350 °C are presented in Fig. 5, while the corresponding flame images were shown in Fig. 4. The most characteristic three radicals of hydrocarbon flames, i.e., OH*, CH*, and C_2* are highlighted; however, the spectra were checked for numerous other potential chemiluminescent peaks, summarized by Gaydon [53]. The black body radiation of D and B25 is spectacular in Fig. 5a, while B75 in Fig. 5b was not a straight flame, hence, the spectrum is practically the dark current. C_2* has the lowest intensity among the highlighted radicals, which fades into the background noise in several cases. This is also true for CH*; B25 showed the lowest intensity at 431 nm, and it also faded into the background in a few cases. Only the OH* was characterized by a high enough signal-to-noise ratio to evaluate and compare the signal with other operational parameters.

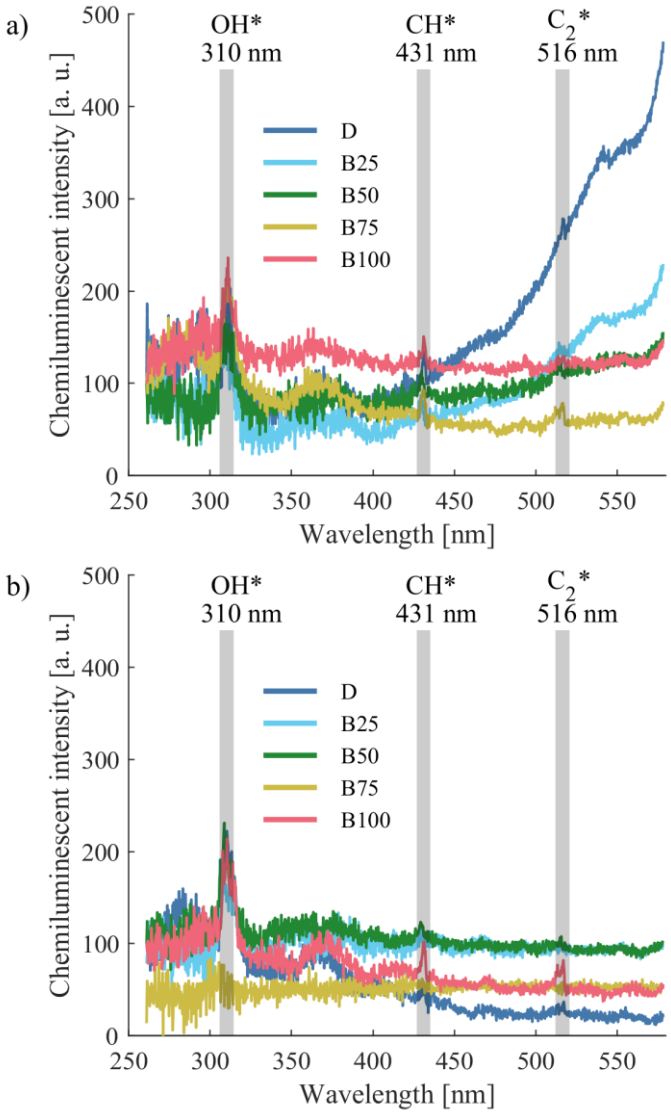

Figure 5. Chemiluminescent emission at a) p_g = 0.3 bar, t_{ca} = 200 °C, b) p_g = 0.9 bar, t_{ca} = 350 °C for all fuels.

Figure 6 contains OH*, flue gas temperature, NO, and CO emission plots at all conditions. The OH* emission was evaluated only for straight flames not due to the fixed spectrometer position, but the signal intensity was very low and fluctuating for distributed combustion mode, leading poor signal-to-noise ratio. The correlation between all the OH*, flue gas temperature, and the NO emission is evident; t_{ca} has a dominating effect and the decrease of overall air temperature with the increasing p_g, notably influences it. The trends apart of OH* plots are continuous, and there is no sudden change within a single combustion mode. The highest values were measured at D combustion, however, all of the other fuels showed similar

amplitudes and maxima. Considering the trends of D and B25, the increasing preheating temperature increases the OH* intensity up to 300 °C and 250 °C, respectively. Then the intensity decreases as fuel evaporation intensifies with a further increase in $t_{ca,}$ which ultimately leads to a more homogeneous fuel-air mixture.

The flue gas temperature, t_{fg}, was governed by t_{ca} and also influenced by the atomizing air temperature, t_{aa}, as it was presented in Fig. 2b, and also affected by the flame shape, shown in Fig. 3. In addition to the thermal boundary conditions, t_{fg} was also affected by thermal radiation in the case of luminous flames. This is especially true for D flames as it showed a high tendency to soot formation, also indicated in Fig. 5a. However, the governing heat transfer mode was convection in distributed combustion mode as the flame luminosity, hence thermal radiation significantly decreased.

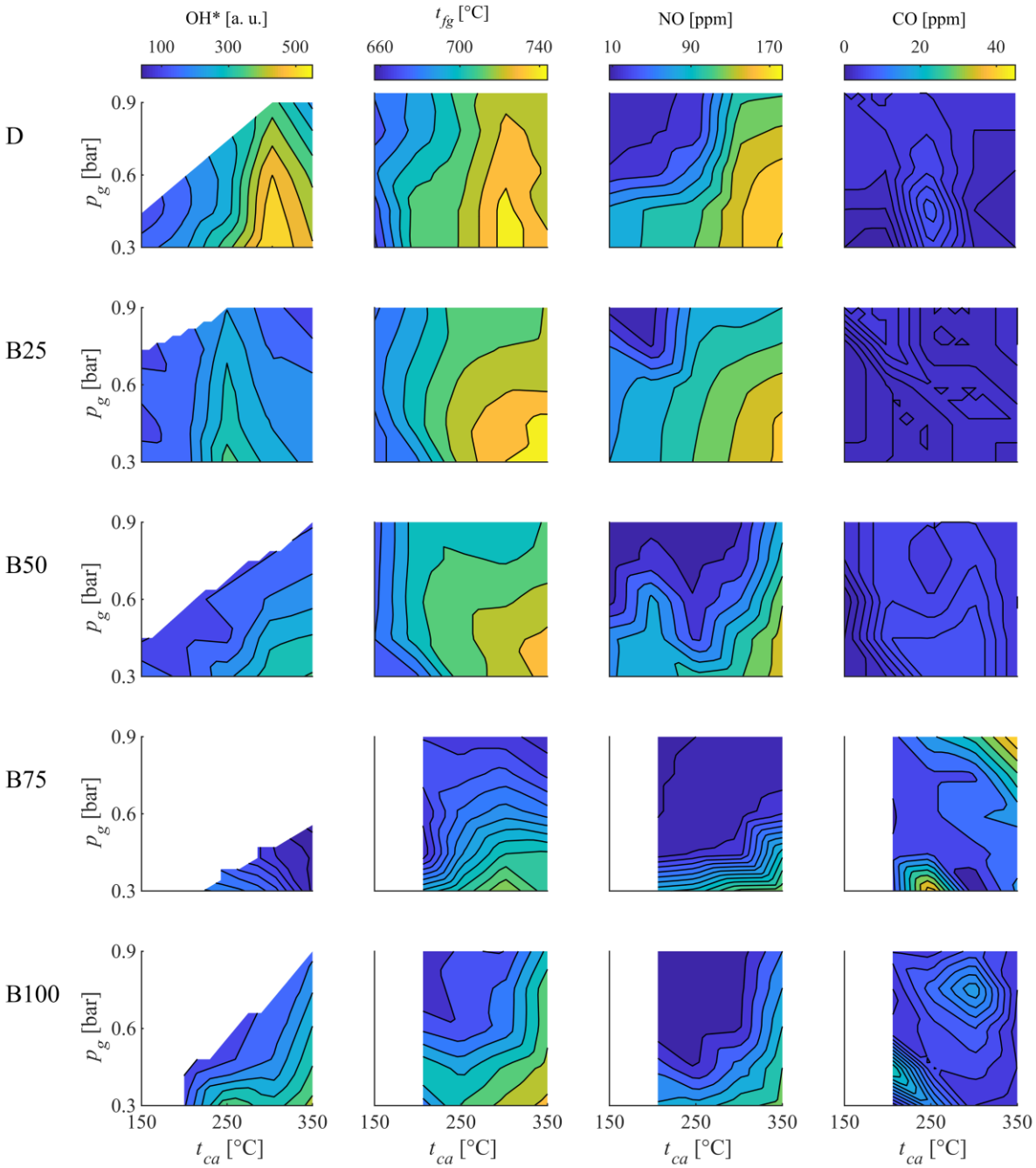

Figure 6. OH* emission, flue gas temperature and pollutant emission results.

NO emission responds most sensitively to the flame shape variation, hence, the suddenly dropping values are clearly limited by the 20 ppm contour lines. These emission trends are closely following the average air temperature variation of Fig. 2b in the case of straight flames. The MTC mode is characterized by ultra-low NO emission, the aforementioned 20 ppm limitation at 4.2% O_2 level is equivalent to 21 ppm NO at 3% O_2 level and 7 ppm at 15% O_2 level. The lowest measured value was 7 ppm which is 2.5 ppm at 15% O_2 level. The

2015/2193/EU directive allows 100 mg/Nm^3 emission, equivalent to 53.1 ppm for natural gas combustion at 3% O_2, which was flawlessly met. Also, this is a conservative comparison since liquid fuel combustion usually has two times higher limitations. The 7 ppm also meets the single cycle, natural gas-fired gas turbine requirement of the BACT Guidelines Part D, which is known as the 'California standard' that is among the strictest ones among all the emission regulations for power plants and utility boilers. This low emission value can only be achieved by using selective catalytic reduction units in existing plants. The critical advantage of the MTC mode is the low average flue gas temperature, which is extremely important for, e.g., gas turbine applications. Even though the temperature is significantly higher in large combustion chambers, the combustion occurring in a large volume is favorable to avoid uneven temperature distribution in the combustion chamber that leads to high NO emission. This mode is facilitated by the following phenomena. Thermodynamically, there is a closely adiabatic expansion in the atomizer nozzle which leads to a sudden temperature drop; this process and the calculation methods were described in an earlier paper [52]. Starting from t_{aa} = 20 °C, the temperature decreases to -1 °C – -29 °C at p_g = 0.3–0.9 bar. The corresponding discharge velocity range is 241–547 m/s. This free jet quickly decays, nevertheless, due to the considerable flow rate, this environment obstructs the fast mixing of the droplets with the hot combustion air, leading to delayed evaporation and hence ignition. This complex behavior will be numerically analyzed as subsequent research work. Nevertheless, the detailed spatial distribution has a notable impact on the flame characteristics, which cannot be directly derived from the global results of Fig. 2b. Overall, the NO emission is decreasing with the increasing share of CME which was also observed by Liu et al. [19] and Chiong et al. [22]. Quantitatively, the NO emission of D combustion was 10% of that of an LPP burner [54], investigated by the authors under highly similar conditions. The significant NO reduction is also evident when straight flames and the MTC mode is compared.

The CO emission was below 10 ppm in the case of D, B25, and B50 combustion. A few measurement points exceeding 20 ppm was observed for B75 and B100 in the transitory operation, i.e., when the flame was altered between straight and distributed combustion modes. Also, atomizing pressures of 0.75 bar and 0.9 bar increased the CO emission of B75 combustion at t_{ca} = 300 and 350 °C, probably due to the poor mixture quality, originated from the high p_g value that resulted in lower residence times. Neat D is characterized by lower CO emission than that of CME combustion, in line with literature data [19,22]. Considering the 2015/2193/EU directive for CO emission of 100 mg/Nm^3 or 87.3 ppm at 3% O_2 level, all the operating points fulfill this limitation. Note that this is respective to natural gas combustion, and the directive allows higher emissions for liquid fuels; consequently, a conservative approach was applied here. The CO emission limitation in BACT Guidelines Part D is 6 ppm at 15% O_2 which is equal to 15 ppm at the currently used 4.2% O_2 level. Figure 6 shows that there is no correlation between the flue gas temperature plots and the increased CO emission, which is a precursor of increasing unburnt hydrocarbon emission [26], confirmed by a preceding study by using a similar burner [54]. Consequently, the MTC burner design is appropriate from CO emission point of view.

Considering the fuels, D featured the lowest CO and the highest NO emission, by comparing similar flame shapes. Since the CO emission was uniformly low in each case compared to the present regulations, NO emission is of greater concern. It was also concluded here that the higher CME share leads to lower NO, in accordance with the literature [22]. It is due to the fuel-bonded oxygen content of CME lowers the *LHV*, hence, the adiabatic flame temperature. The MTC mode was the dominant one in the case of B75, followed by B100 and B50. Interestingly, distributed combustion was present in a significantly wider parameter range of D combustion than in the case of B25. Consequently, the high share of biodiesel is favorable, and less concentrated fuels are advised to be tested before direct use since the combustion

characteristics might notably differ even though the physical properties are close to that of neat D.

4. Conclusions

Combustion of standard diesel fuel (D, EN590:2017), coconut methyl ester (CME), and their blends were investigated in a novel, ultra-low emission burner. The notable ignition delaying effect of the low temperature atomizing air on the combustion process and flame characteristic lead to the name of Mixture Temperature-Controlled (MTC) Combustion, which can be used in numerous steady-operating practical applications, including gas turbines, furnaces, and boilers. MTC provided significantly lower emissions than current combustion concepts, such as LPP. The following conclusions were derived.

1. The CO emission was below 10 ppm in most of the cases, which is equivalent to 12 and 4 mg/Nm^3 at 3% and 15% O_2, respectively, fulfilling all the regulations.
2. The NO emission of straight flames ranged from 60 to 183 ppm, exceeding the limitations of the 2015/2193/EU directive of 100 mg/Nm^3 or 53.1 ppm at 3% O_2. Nevertheless, the emission at MTC mode was < 20 ppm in the majority of the cases that is equivalent to 40 mg/Nm^3 at 3% O_2, and 13 mg/Nm^3 at 15% O_2. The lowest measured NO emission value was 7 ppm (2.5 ppm at 15% O_2), fulfilling the 'California standard' for single-cycle gas turbines. Also, this pollutant concentration was only 10% of that of an LPP burner operated under similar conditions [54].
3. Only the chemiluminescent emission of OH* of the straight flames provided an acceptable signal-to-noise ratio. The trends followed that of both flue gas temperature and NO emission.
4. Overall, the combustion of B100 provided the lowest emissions, while blends with lower CME share leads to higher emissions.

Funding

This work has been supported by the National Research, Development and Innovation Fund of Hungary, project №.s OTKA-FK 124704, TUDFO/51757/2019-ITM Thematic Excellence Program, New National Excellence Program of the Ministry for Innovation and Technology, project №.s ÚNKP-19-4-BME-213, ÚNKP-19-3-I-BME-243, and the János Bolyai Research Scholarship of the Hungarian Academy of Sciences.

Conflict of interest

The authors declare that there is no conflict of interest.

References

[1] Bolwig S, Bazbauers G, Klitkou A, Lund PD, Blumberga A, Gravelsins A, et al. Review of modelling energy transitions pathways with application to energy system flexibility. Renew Sustain Energy Rev 2019;101:440–52. doi:10.1016/j.rser.2018.11.019.

[2] Du Z, Wood DL, Belharouak I. Enabling fast charging of high energy density Li-ion cells with high lithium ion transport electrolytes. Electrochem Commun 2019;103:109–13. doi:10.1016/j.elecom.2019.04.013.

[3] Mao M, Gao T, Hou S, Wang F, Chen J, Wei Z, et al. High-Energy-Density Rechargeable Mg Battery Enabled by a Displacement Reaction. Nano Lett 2019;19:6665–72. doi:10.1021/acs.nanolett.9b02963.

[4] Shi W, Mao J, Xu X, Liu W, Zhang L, Cao X, et al. An ultra-dense NiS2/reduced graphene oxide composite cathode for high-volumetric/gravimetric energy density nickel-zinc batteries. J Mater Chem A 2019;7:15654–61. doi:10.1039/c9ta04900b.

[5] Eggels R. The challenge of modelling aeronautical combustion chambers. Proc. 9th Eur. Combust. Meet., Lisbon: 2019.

[6] Liu G, Yan B, Chen G. Technical review on jet fuel production. Renew Sustain Energy Rev 2013;25:59–70. doi:10.1016/j.rser.2013.03.025.

[7] Matsumoto H, Domae K. Assessment of competitive hub status of cities in Europe and Asia from an international air traffic perspective. J Air Transp Manag 2019;78:88–95. doi:10.1016/j.jairtraman.2019.01.006.

[8] Prussi M, O'Connell A, Lonza L. Analysis of current aviation biofuel technical production potential in EU28. Biomass and Bioenergy 2019;130:105371. doi:10.1016/j.biombioe.2019.105371.

[9] Chiong MC, Chong CT, Ng JH, Lam SS, Tran MV, Chong WWF, et al. Liquid biofuels production and emissions performance in gas turbines: A review. Energy Convers Manag 2018;173:640–58. doi:10.1016/j.enconman.2018.07.082.

[10] Wei H, Liu W, Chen X, Yang Q, Li J, Chen H. Renewable bio-jet fuel production for aviation: A review. Fuel 2019;254. doi:10.1016/j.fuel.2019.06.007.
[11] Wong KY, Ng JH, Chong CT, Lam SS, Chong WT. Biodiesel process intensification through catalytic enhancement and emerging reactor designs: A critical review. Renew Sustain Energy Rev 2019;116. doi:10.1016/j.rser.2019.109399.
[12] IEA. Technology roadmap: Delivering sustainable Bioenergy. 2017.
[13] Committee on Industry Research and Energy. Report on the proposal for a directive of the European Parliament and of the Council on the promotion of the use of energy from renewable sources (recast (COM(2016)0767 – C8-0500/2016 – 2016/0382(COD)). 2017.
[14] Lokesh K, Sethi V, Nikolaidis T, Goodger E, Nalianda D. Life cycle greenhouse gas analysis of biojet fuels with a technical investigation into their impact onjet engine performance. Biomass and Bioenergy 2015;77:26–44. doi:10.1016/j.biombioe.2015.03.005.
[15] European Union Aviation Safety Agency. European Aviation Environmental Report. 2019.
[16] Why ESK, Ong HC, Lee HV, Gan YY, Chen WH, Chong CT. Renewable aviation fuel by advanced hydroprocessing of biomass: Challenges and perspective. Energy Convers Manag 2019;199:112015. doi:10.1016/j.enconman.2019.112015.
[17] KLM. Corporate Biofuel Programme 2019. https://www.klm.com/travel/nl_en/prepare_for_travel/fly_co2_neutral/all_about_sustainable_travel/biofuel.htm (accessed January 16, 2020).
[18] Bergthorson JM, Thomson MJ. A review of the combustion and emissions properties of advanced transportation biofuels and their impact on existing and future engines. Renew Sustain Energy Rev 2015;42:1393–417. doi:10.1016/j.rser.2014.10.034.
[19] Liu K, Wood JP, Buchanan ER, Martin P, Sanderson VE. Biodiesel as an Alternative Fuel in Siemens Dry Low Emissions Combustors: Atmospheric and High Pressure Rig Testing. J Eng Gas Turbines Power 2010;132:1–9. doi:10.1115/1.3204617.
[20] Bolszo CD, McDonell VG. Emissions optimization of a biodiesel fired gas turbine. Proc Combust Inst 2009;32:2949–56. doi:10.1016/j.proci.2008.07.042.
[21] Chong CT, Chiong M, Ng J, Lim M, Tran M-V, Valera-Medina A, et al. Oxygenated sunflower biodiesel: Spectroscopic and emissions quantification under reacting swirl spray conditions. Energy 2019;178:804–13. doi:10.1016/j.energy.2019.04.201.
[22] Chiong MC, Chong CT, Ng JH, Tran MV, Lam SS, Valera-Medina A, et al. Combustion and emission performances of coconut, palm and soybean methyl esters under reacting spray flame conditions. J Energy Inst 2019;92:1034–44. doi:10.1016/j.joei.2018.07.003.
[23] Correa SM. Power generation and aeropropulsion gas turbines: From combustion science to combustion technology. Symp Combust 1998;27:1793–807. doi:10.1016/S0082-0784(98)80021-0.
[24] Zhou H, Meng S. Numerical prediction of swirl burner geometry effects on NOx emission and combustion instability in heavy oil-fired boiler. Appl Therm Eng 2019;159:113843. doi:10.1016/j.applthermaleng.2019.113843.
[25] Gupta AK. Gas Turbine Combustion: Prospects and Challenges. Energy Convers Manag 1997;38:1311–8.
[26] Lefebvre AH, Ballal DR. Gas turbine combustion. third. Boca Raton: CRC Press; 2010. doi:10.1002/1521-3773.
[27] Guin C, Trichet P. Optimisation of a two-head lean prevaporised premixed combustor. Aerosp Sci Technol 2004;8:35–46. doi:10.1016/j.ast.2003.09.007.
[28] Beér JM, Chigier NA. Combustion aerodynamics. London: Robert E. Krieger

Publishing Company, Inc.; 1972.
[29] Huang Y, Yang V. Dynamics and stability of lean-premixed swirl-stabilized combustion. Prog Energy Combust Sci 2009;35:293–364. doi:10.1016/j.pecs.2009.01.002.
[30] Liu Y, Sun X, Sethi V, Nalianda D, Li YG, Wang L. Review of modern low emissions combustion technologies for aero gas turbine engines. Prog Aerosp Sci 2017;94:12–45. doi:10.1016/j.paerosci.2017.08.001.
[31] Wang Z, Lin Y, Wang J, Zhang C, Peng Z. Experimental study on NOx emission correlation of fuel staged combustion in a LPP combustor at high pressure based on NO-chemiluminescence. Chinese J Aeronaut 2019;33:550–60. doi:10.1016/j.cja.2019.09.004.
[32] Reay DA. Catalytic combustion: Current status and implications for energy efficiency in the process industries. Heat Recover Syst CHP 1993;13:383–90. doi:10.1016/0890-4332(93)90039-X.
[33] Jovanović R, Swiatkowski B, Kakietek S, Škobalj P, Lazović I, Cvetinović D. Mathematical modelling of swirl oxy-fuel burner flame characteristics. Energy Convers Manag 2019;191:193–207. doi:10.1016/j.enconman.2019.04.027.
[34] Wu XD, Yang Q, Chen GQ, Hayat T, Alsaedi A. Progress and prospect of CCS in China: Using learning curve to assess the cost-viability of a 2×600 MW retrofitted oxyfuel power plant as a case study. Renew Sustain Energy Rev 2016;60:1274–85. doi:10.1016/j.rser.2016.03.015.
[35] Xing F, Kumar A, Huang Y, Chan S, Ruan C, Gu S, et al. Flameless combustion with liquid fuel: A review focusing on fundamentals and gas turbine application. Appl Energy 2017;193:28–51. doi:10.1016/j.apenergy.2017.02.010.
[36] Fooladgar E, Tóth P, Duwig C. Characterization of flameless combustion in a model gas turbine combustor using a novel post-processing tool. Combust Flame 2019;204:356–67. doi:10.1016/j.combustflame.2019.03.015.
[37] Yang W, Wang B, Lei S, Wang K, Chen T, Song Z, et al. Combustion optimization and NOx reduction of a 600 MWe down-fired boiler by rearrangement of swirl burner and introduction of separated over-fire air. J Clean Prod 2019;210:1120–30. doi:10.1016/j.jclepro.2018.11.077.
[38] Zhou C, Wang Y, Jin Q, Chen Q, Zhou Y. Mechanism analysis on the pulverized coal combustion flame stability and NOx emission in a swirl burner with deep air staging. J Energy Inst 2019;92:298–310. doi:10.1016/j.joei.2018.01.006.
[39] Ti S, Chen Z, Li Z, Kuang M, Xu G, Lai J, et al. Influence of primary air cone length on combustion characteristics and NOx emissions of a swirl burner from a 0.5 MW pulverized coal-fired furnace with air staging. Appl Energy 2018;211:1179–89. doi:10.1016/j.apenergy.2017.12.014.
[40] Ferri A. Mixing-Controlled Supersonic Combustion. Annu Rev Fluid Mech 1973;5:301–38. doi:10.1146/annurev.fl.05.010173.001505.
[41] Katrašnik T. An advanced real-time capable mixture controlled combustion model. Energy 2016;95:393–403. doi:10.1016/j.energy.2015.11.066.
[42] Wang Q, Chen Z, Wang L, Zeng L, Li Z. Application of eccentric-swirl-secondary-air combustion technology for high-efficiency and low-NOx performance on a large-scale down-fired boiler with swirl burners. Appl Energy 2018;223:358–68. doi:10.1016/j.apenergy.2018.04.064.
[43] Channiwala SA, Parikh PP. A unified correlation for estimating HHV of solid, liquid and gaseous fuels. Fuel 2002;81:1051–63. doi:10.1016/S0016-2361(01)00131-4.
[44] Kanaveli IP, Atzemi M, Lois E. Predicting the viscosity of diesel/biodiesel blends. Fuel 2017;199:248–63. doi:10.1016/j.fuel.2017.02.077.

[45] Ayetor GK, Sunnu A, Parbey J. Effect of biodiesel production parameters on viscosity and yield of methyl esters: Jatropha curcas, Elaeis guineensis and Cocos nucifera. Alexandria Eng J 2015;54:1285–90. doi:10.1016/j.aej.2015.09.011.
[46] Das M, Sarkar M, Datta A, Santra AK. Study on viscosity and surface tension properties of biodiesel-diesel blends and their effects on spray parameters for CI engines. Fuel 2018;220:769–79. doi:10.1016/j.fuel.2018.02.021.
[47] Poling BE, Prausnitz JM, O'Connell JP. The properties of gases and liquids. Fifth. McGraw-Hill; 2001. doi:10.1036/0070116822.
[48] Urbán A, Malý M, Józsa V, Jedelský J. Effect of liquid preheating on high-velocity airblast atomization: From water to crude rapeseed oil. Exp Therm Fluid Sci 2019;102:137–51. doi:10.1016/j.expthermflusci.2018.11.006.
[49] Al Qubeissi M, Sazhin SS, Elwardany AE. Modelling of blended Diesel and biodiesel fuel droplet heating and evaporation. Fuel 2017;187:349–55. doi:10.1016/j.fuel.2016.09.060.
[50] Al Qubeissi M. Predictions of droplet heating and evaporation: An application to biodiesel, diesel, gasoline and blended fuels. Appl Therm Eng 2018;136:260–7. doi:10.1016/j.applthermaleng.2018.03.010.
[51] Józsa V, Kun-Balog A. Stability and emission analysis of crude rapeseed oil combustion. Fuel Process Technol 2017;156:204–10. doi:10.1016/j.fuproc.2016.11.004.
[52] Urbán A, Zaremba M, Malý M, Józsa V, Jedelský J. Droplet dynamics and size characterization of high-velocity airblast atomization. Int J Multiph Flow 2017;95:1–11. doi:10.1016/j.ijmultiphaseflow.2017.02.001.
[53] Gaydon AG. The spectroscopy of flames. 2nd ed. Chapman and Hall Ltd., London; 1974. doi:10.1016/0010-2180(75)90098-X.
[54] Kun-Balog A, Sztankó K, Józsa V. Pollutant emission of gaseous and liquid aqueous bioethanol combustion in swirl burners. Energy Convers Manag 2017;149:896–903. doi:10.1016/j.enconman.2017.03.064.